eLIFE elifesciences.org

SHORT REPORT

Figures and figure supplements

High resolution cryo-EM structure of the helical RNA-bound Hantaan virus nucleocapsid reveals its assembly mechanisms

Benoît Arragain *et al*

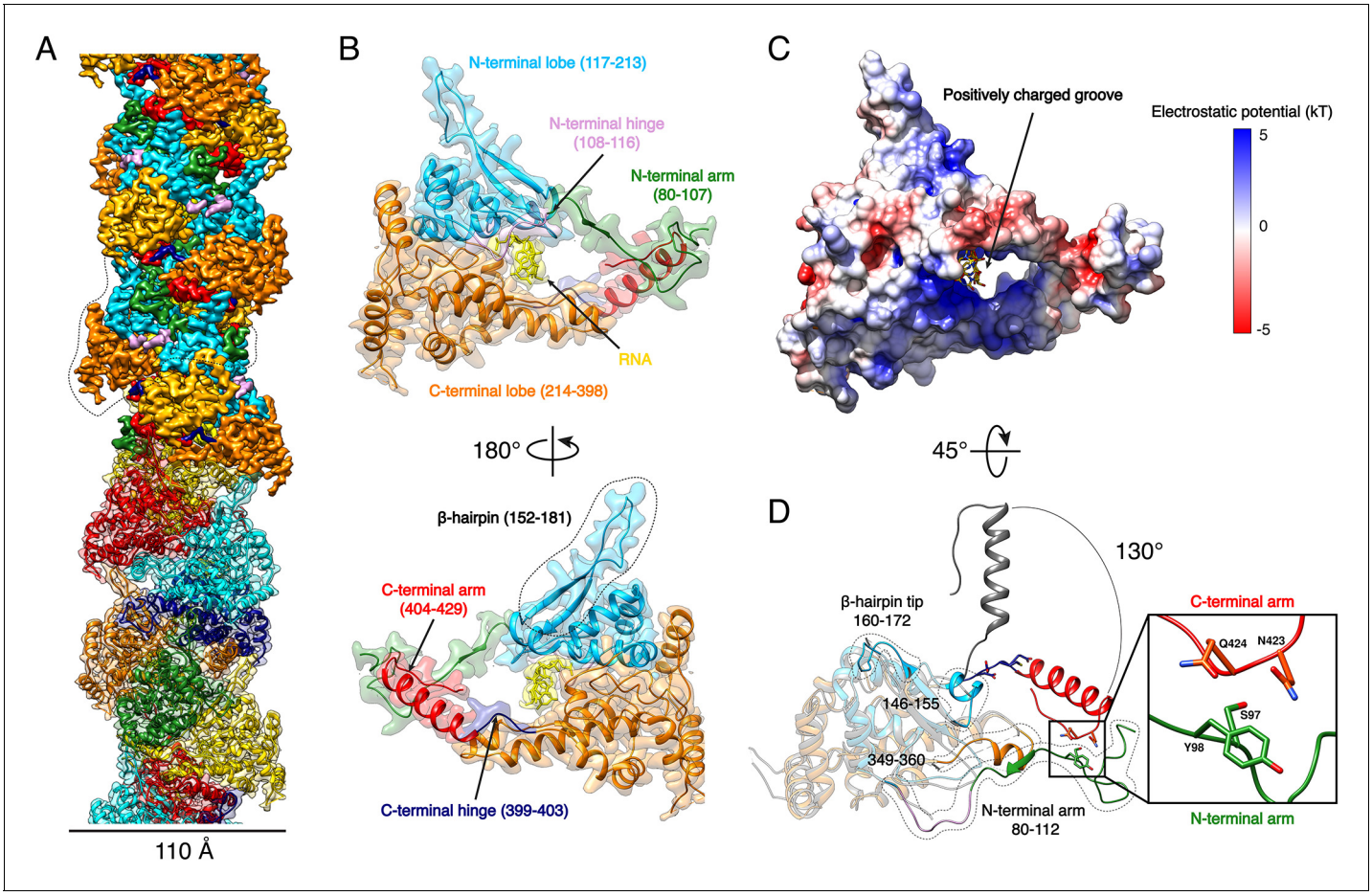

Figure 1. HTNV-NC structure. (**A**) HTNV-NC helical organisation. The upper part of the cryo-EM map is coloured per NP domain, whereas the lower part is shown as transparent and coloured per NP protomer. The NP surrounded by dotted lines corresponds to ***Figure 1B*** orientation. (**B**) Domain organisation of one monomer extracted from the NC helical assembly. Each domain is coloured as in ***Figure 1A*** upper part. The newly described β-hairpin (residues 152–181) is labelled and surrounded by dotted lines. (**C**) Electrostatic surface representation of HTNV-NP monomer. (**D**) Superimposition of monomeric NP_{core} (***Olal and Daumke, 2016***) (in gray) and NP from the present structure (coloured as in ***Figure 1A,B***). The Ct_{arm} rotation is highlighted and newly built elements are labelled, shown as non-transparent and surrounded by dotted lines. A close up view of the Ct_{arm}/Nt_{arm} interaction is shown.

DOI: https://doi.org/10.7554/eLife.43075.003

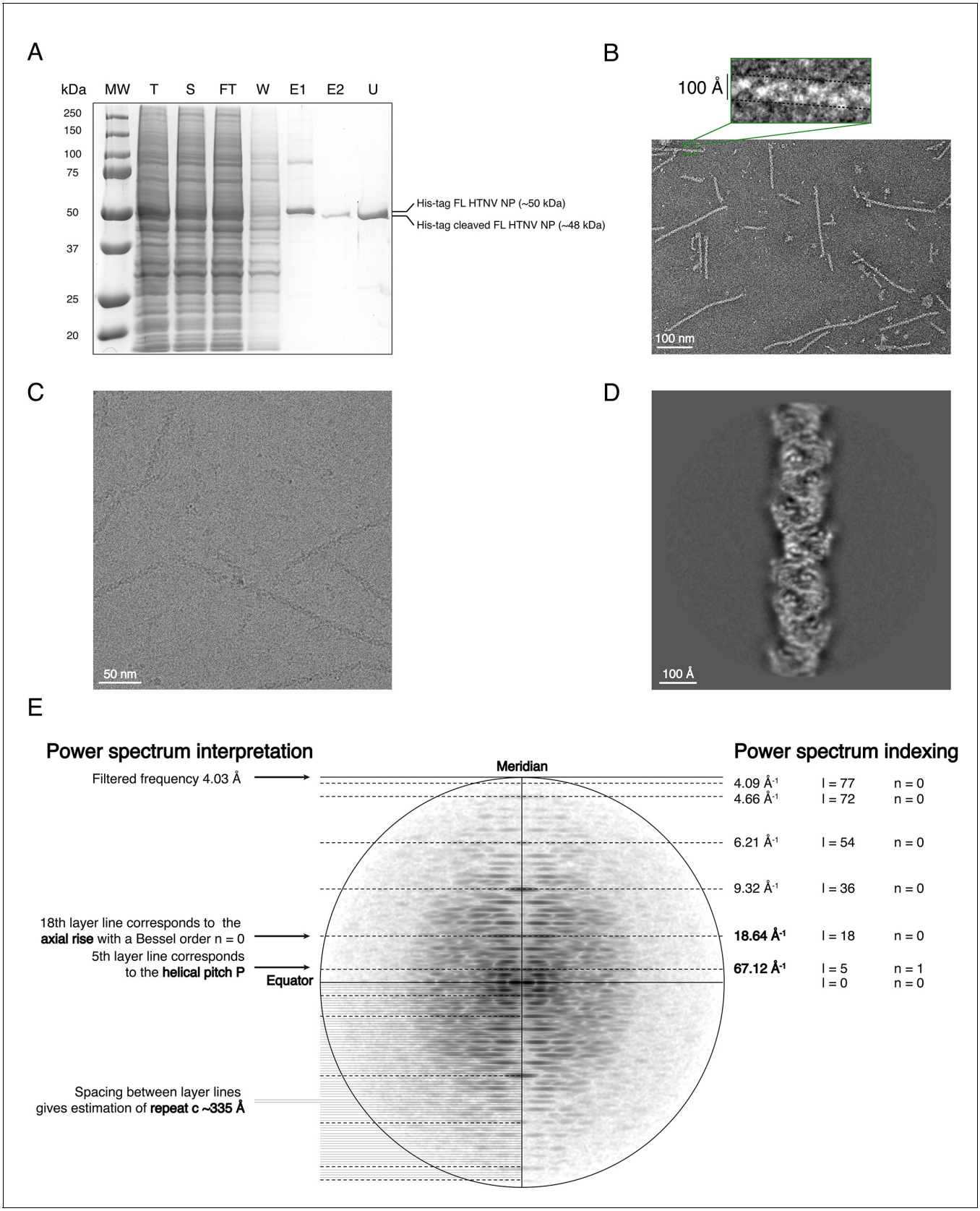

Figure 1—figure supplement 1. Purification, EM analysis and symmetry determination of HTNV-NC. (**A**) SDS-PAGE gel of HTNV-NC purification. T: total fraction, S: soluble fraction, FT: flow through of the 1st Ni-NTA purification, W: wash of the 1st Ni-NTA purification, E1: elution of the 1st Ni-NTA

Figure 1—figure supplement 1 continued on next page

Figure 1—figure supplement 1 continued

purification, E2: supernatant after TEV cleavage and 2nd Ni-NTA purification, U: concentrated protein after ultra-centrifugation. (**B**,**C**) Negative stain (**B**) and cryo electron micrographs (**C**) of HTNV-NC. Scale bar is indicated. (**D**) 2D class average. (**E**) 2D class average power spectrum, indexing and interpretation enabling symmetry determination.

DOI: https://doi.org/10.7554/eLife.43075.004

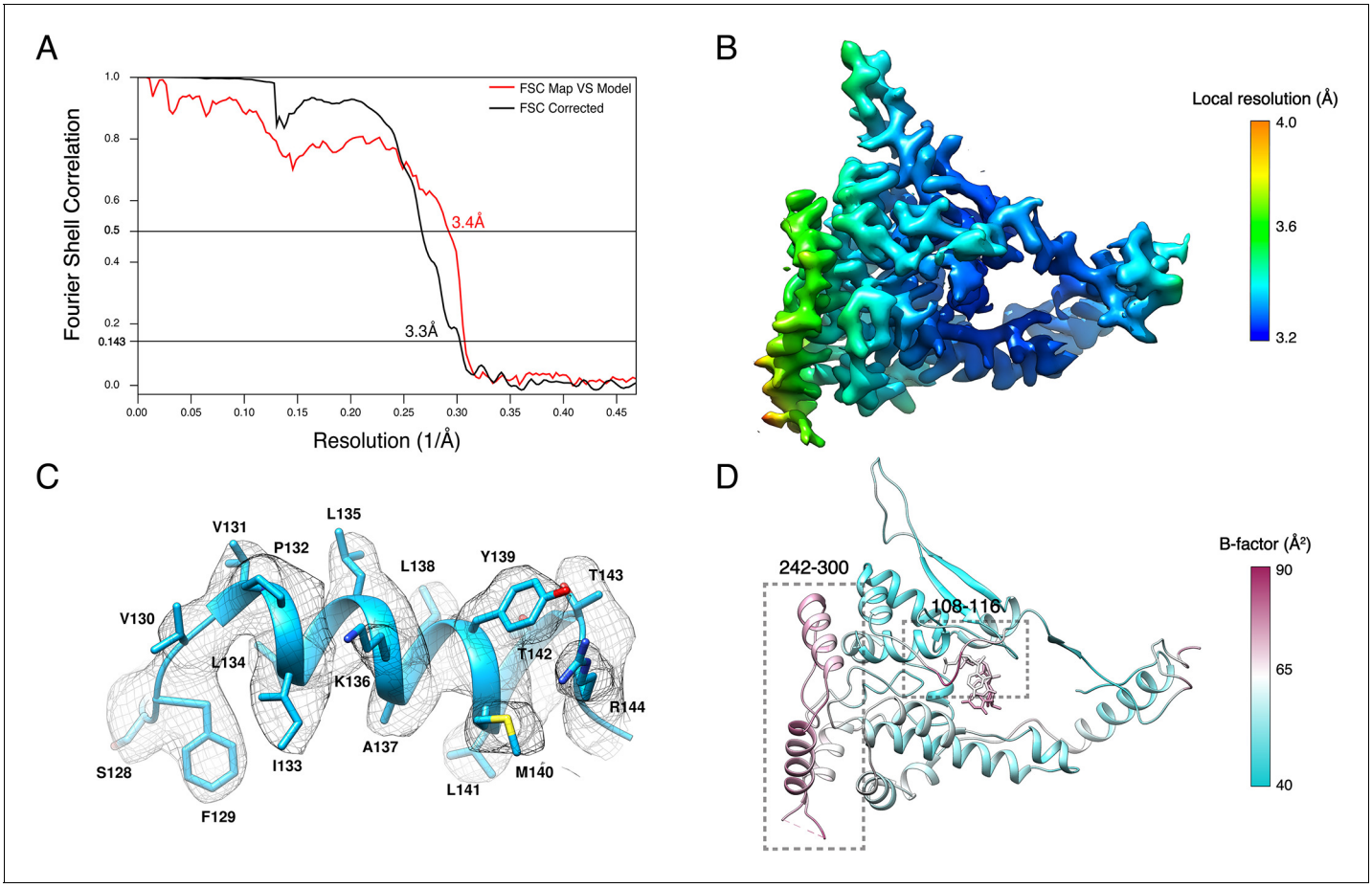

Figure 1—figure supplement 2. Resolution of HTNV-NC structure. (**A**) The gold-standard Fourier shell correlation (FSC) of masked map indicates a resolution of 3.3 Å with the FSC = 0.143 criteria. The FSC between the map and the model is 3.4 Å according to FSC = 0.5 criterion. (**B**) Local resolution. (**C**) Zoom-up view of a representative α-helix that shows clear side chains densities illustrating the quality of the map. (**D**) The B-factor analysis strongly correlates with the local resolution analysis (**B**) and shows that the N-terminal hinge and the solvent-exposed region containing residues 242–300 are flexible.

DOI: https://doi.org/10.7554/eLife.43075.005

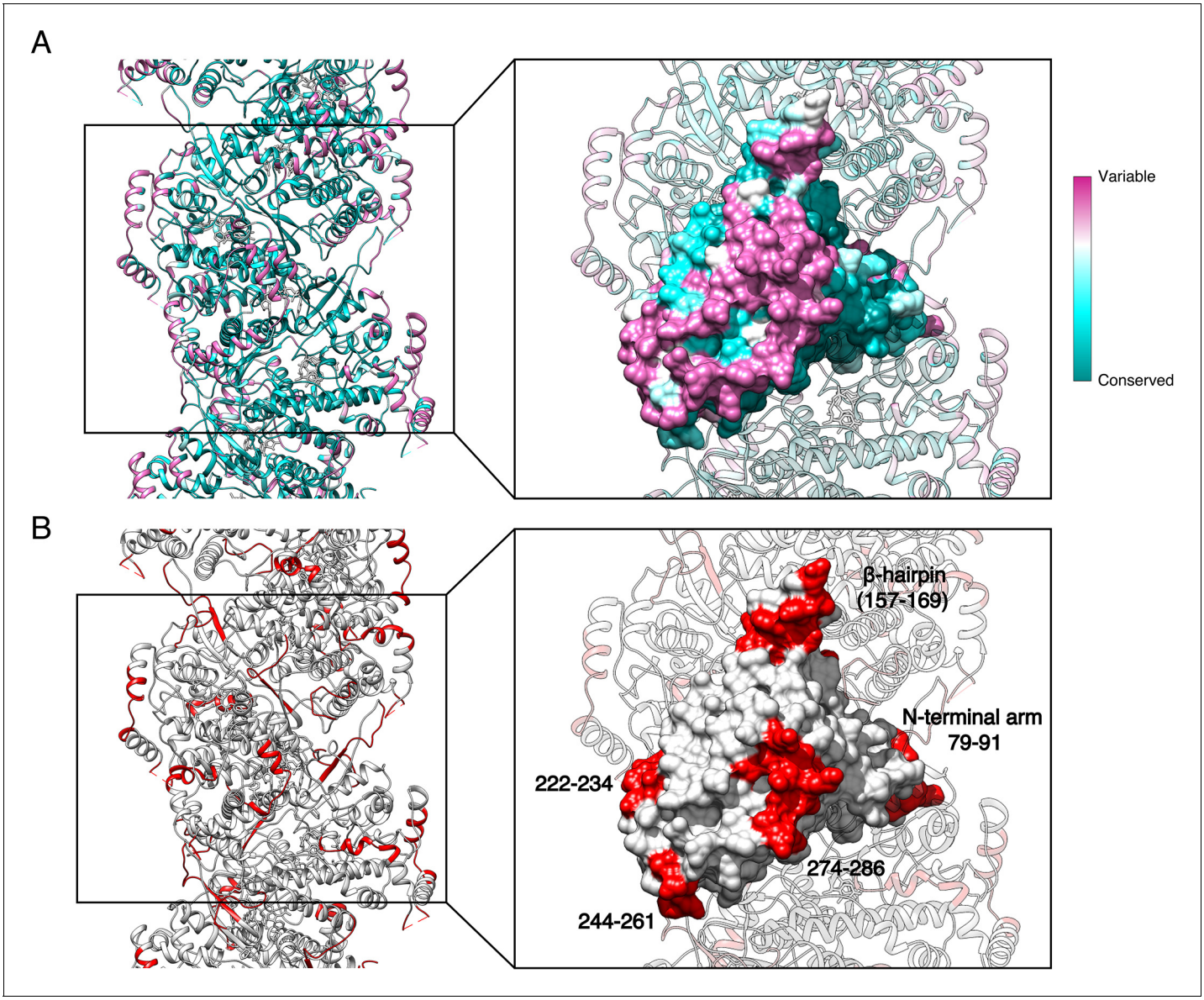

Figure 1—figure supplement 3. Specific antigenic sites are localised in variable regions of the NC surface. (**A**) Surface conservation mapping of HTNV-NC. Regions localised towards NC interior, in particular regions involved in RNA-binding and NP-NP oligomerisation are conserved, whereas HTNV-NC exposed regions are more variable. (**B**) Epitopes involved in serotype-specific and cross-reactive recognition of HTNV-NC determined in (***Tischler et al., 2008***) are shown in red. They correspond to surface-exposed regions of HTNV-NC corroborating their necessary accessibility.

DOI: https://doi.org/10.7554/eLife.43075.006

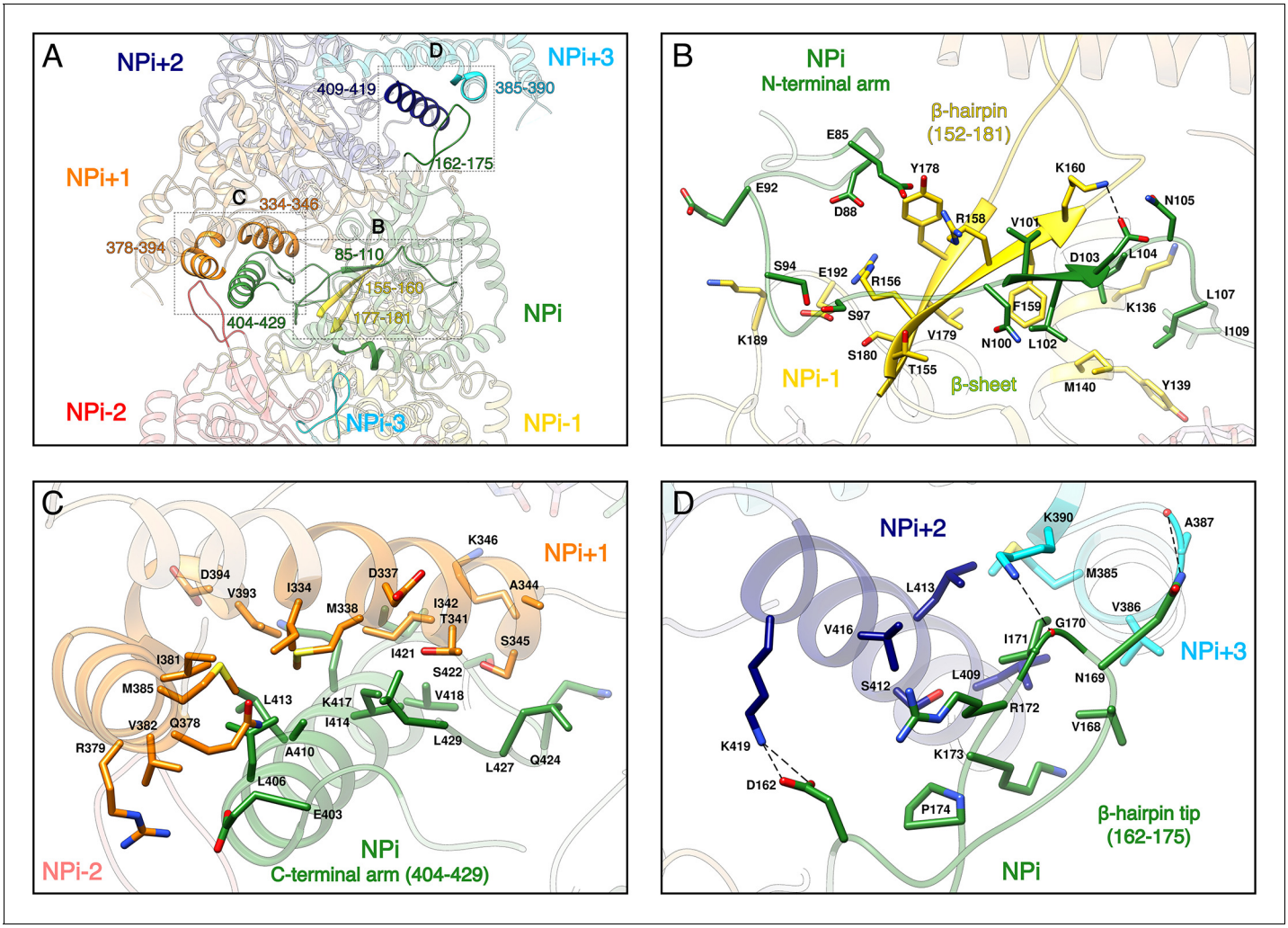

Figure 2. NP-NP interactions. (**A**) General view. The filament orientation corresponds to RNA direction from 5′ to 3′. Each NP protomer is coloured differently. Interacting regions of NP_i with subunits ranging from. NP_{i-3} to NP_{i+3} are shown as non-transparent. Positions of ***Figure 2B,C,D*** close-up views are indicated with dotted lines. (**B**) NP_i Nt_{arm} binding site in NP_{i-1}. Residues 101–103 from NP_i Nt_{arm} form a β-sheet with β-strands 155–160 and 177–181 from NP_{i-1}. Hydrogen bonds are shown as black dotted lines. (**C**) NP_i Ct_{arm} binding site in NP_{i+1}. (**D**) Binding of NP_i β-hairpin tip (residues 162–175) on NP_{i+2} (residues 409–419) and NP_{i+3} (residues 385–390). NP_i I171 is plugged into a hydrophobic pocket formed by L409 and L413 of the NP_{i+2} C-terminal helix and M385 and K390 sidechains of the NP_{i+3} C-terminal lobe. Hydrogen bonds between the residue pairs N169-A387 and G170-K390 from NP_i and NP_{i+3} respectively, further stabilise this interaction contributing to the rigidification of HTNV-NC.

DOI: https://doi.org/10.7554/eLife.43075.009

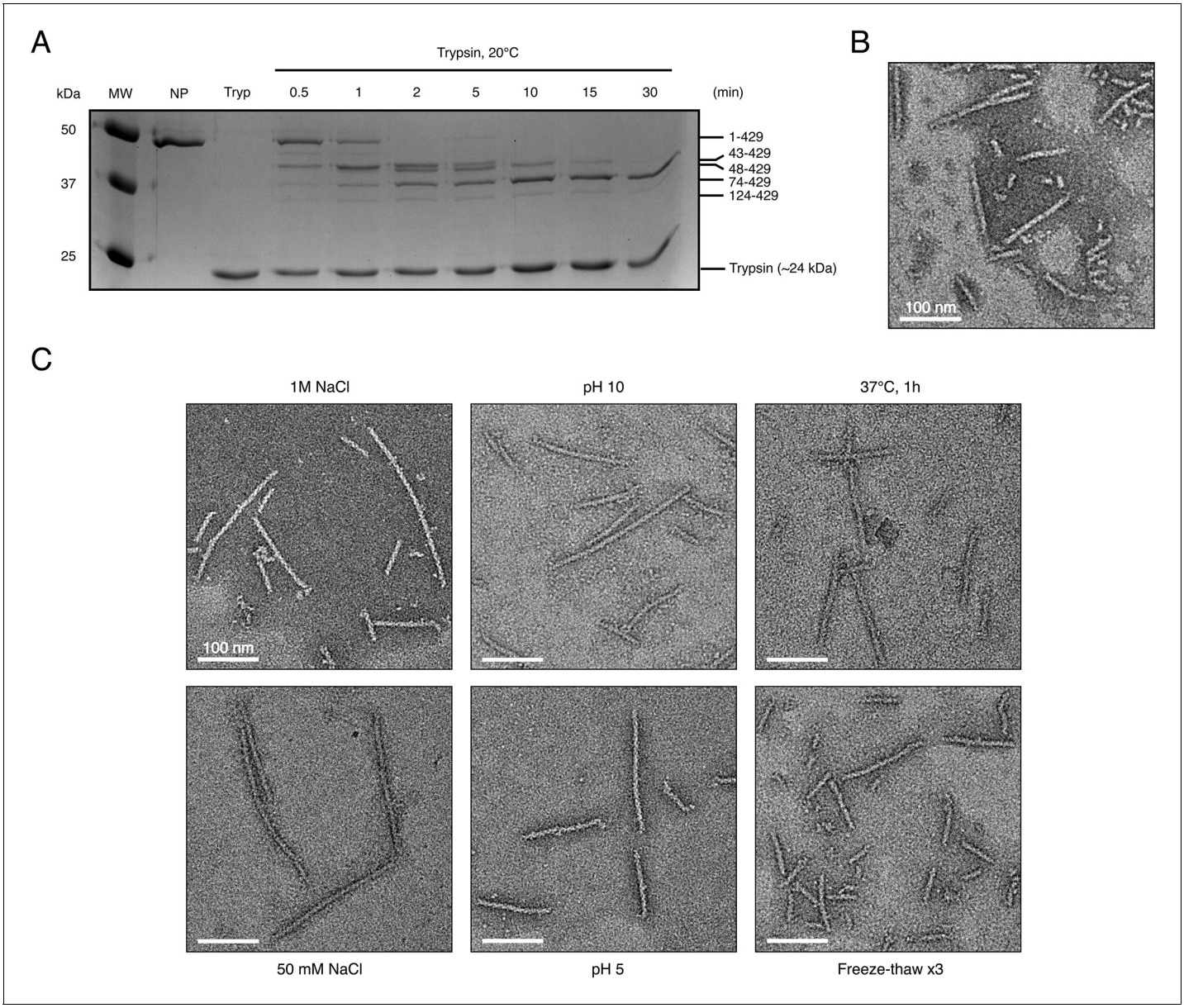

Figure 2—figure supplement 1. Limited proteolysis and stability of recombinant HTNV-NCs. (**A**) SDS-Page analysis of trypsin digested HTNV-NC. MW represents the molecular weight markers. NC were incubated with trypsin (Tryp) at 20°C for different duration from 0 (NP) to 30 min. After 30 min, a stable construct containing residues 74 to 429 is obtained. Presence of intermediate limited proteolysis fragments containing residues 43–429 and 48–429 strongly suggests that the N-terminal residues 1–73 are not disordered and might correspond to a coiled-coil as observed by ***Boudko et al. (2007)***. (**B**) Negative stain EM micrograph of truncated construct $NP_{74\text{-}429}$ displays NC similar to the ones of full-length NP. (**C**) Negative stain micrographs of full-length HTNV-NCs incubated in different pHs and salt concentration as indicated. NC fibers stay stable in harsh conditions. Consecutive freeze-thaw breaks NC in small rigid parts. Scale bars are indicated.

DOI: https://doi.org/10.7554/eLife.43075.010

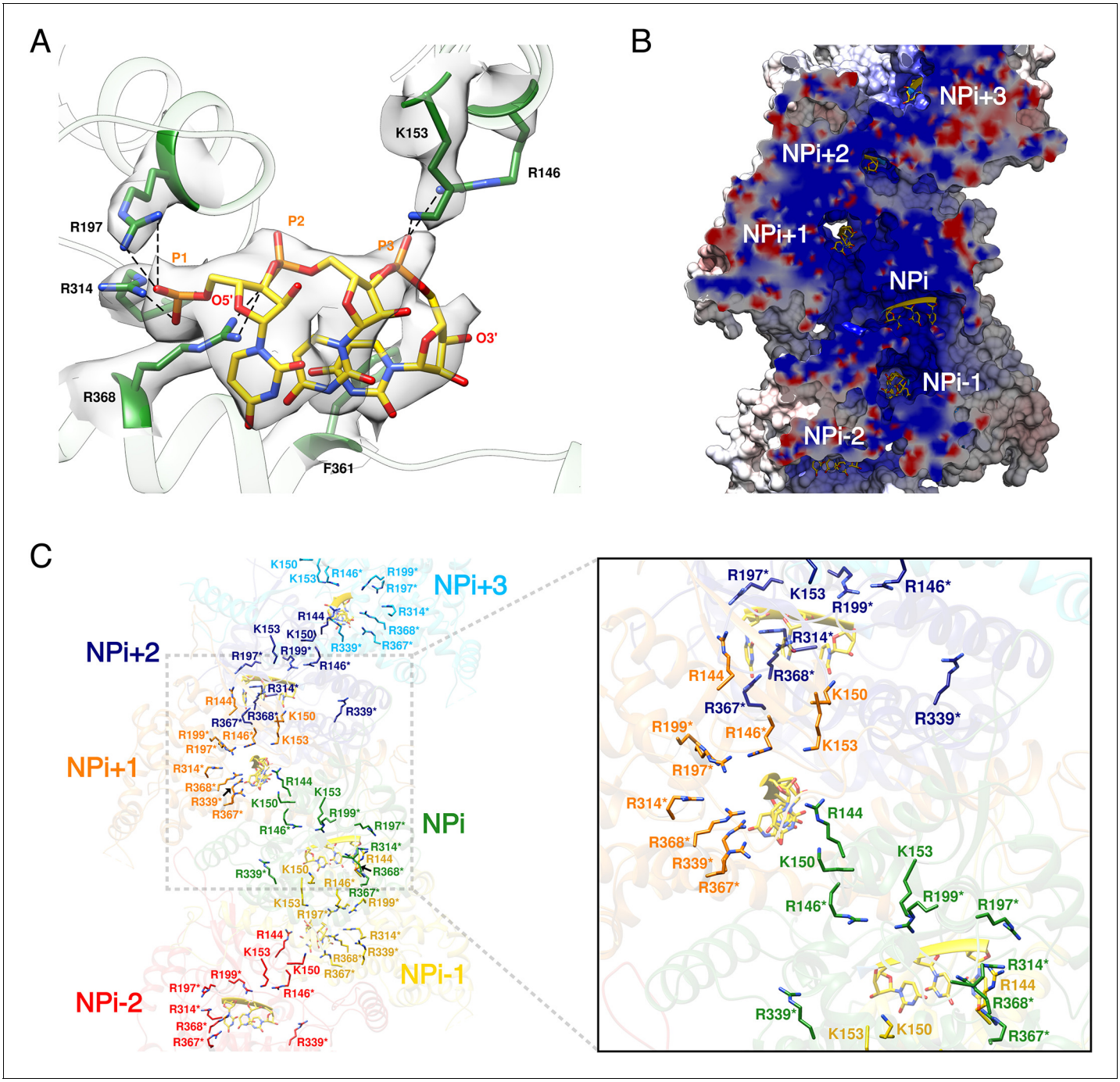

Figure 3. HTNV-NC RNA binding site. (**A**) RNA binding mode of 3 nucleotides. EM density of RNA and RNA-binding residues are displayed in transparent grey. Hydrogen bonds are shown as dotted lines. (**B**) Cut-away view of NC electrostatic potential showing the continuous positively-charged groove. RNA nucleotides are displayed. (**C**) RNA-binding residues are shown as sticks and coloured per subunit. RNA-binding residues defined in ***Guo et al. (2016)***, namely R146*, R197*, R199*, R314*, R339*, R367*, R368* are labelled with stars, while RNA-binding residues identified in the present structure, namely R144, K150, K153 are shown without stars.

DOI: https://doi.org/10.7554/eLife.43075.012

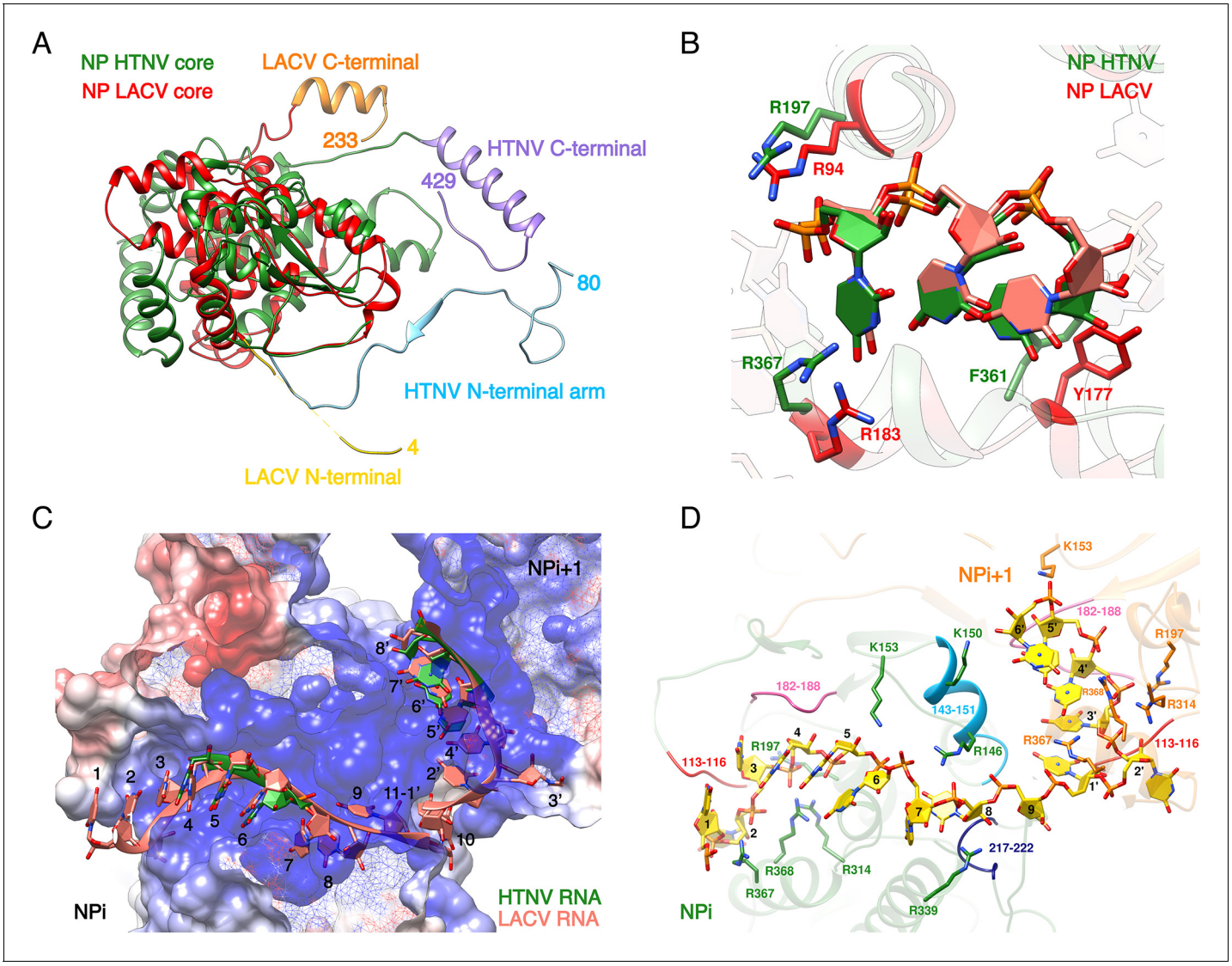

Figure 3—figure supplement 1. Comparison of LACV and HTNV-NP/NC, RNA-binding model. (**A**) Superimposition of HTNV and LACV NP_{cores}. HTNV and LACV Nt_{arms} and Ct_{arms} contain the same secondary structures but LACV arms are significantly shorter and differ in orientation. (**B**) HTNV-NP-bound nucleotides adopt a similar conformation as LACV-NP-bound nucleotides 5 to 7. The nucleotide binding pocket is conserved in HTNV-NP and LACV-NP. (**C**) Cut-away view of HTNV-NC electrostatic potential. Visible HTNV nucleotides are shown in green. LACV nucleotides position based on superimposition of LACV and HTNV NP_{cores} are shown in salmon. LACV RNA fits reasonably well into HTNV-NC RNA path, however LACV nucleotide 11 from NP_i clashes with LACV nucleotide one from NP_{i+1} showing that each HTNV-NP binds less than 11 nucleotides. LACV nucleotides numbering is indicated. (**D**) Model of HTNV-NC bound to nine nucleotides. Nucleotides numbering from 1 to 9 is indicated. Residues interacting with riboses and phosphates are shown as sticks. Regions interacting with bases are coloured and specifically labelled.

DOI: https://doi.org/10.7554/eLife.43075.013

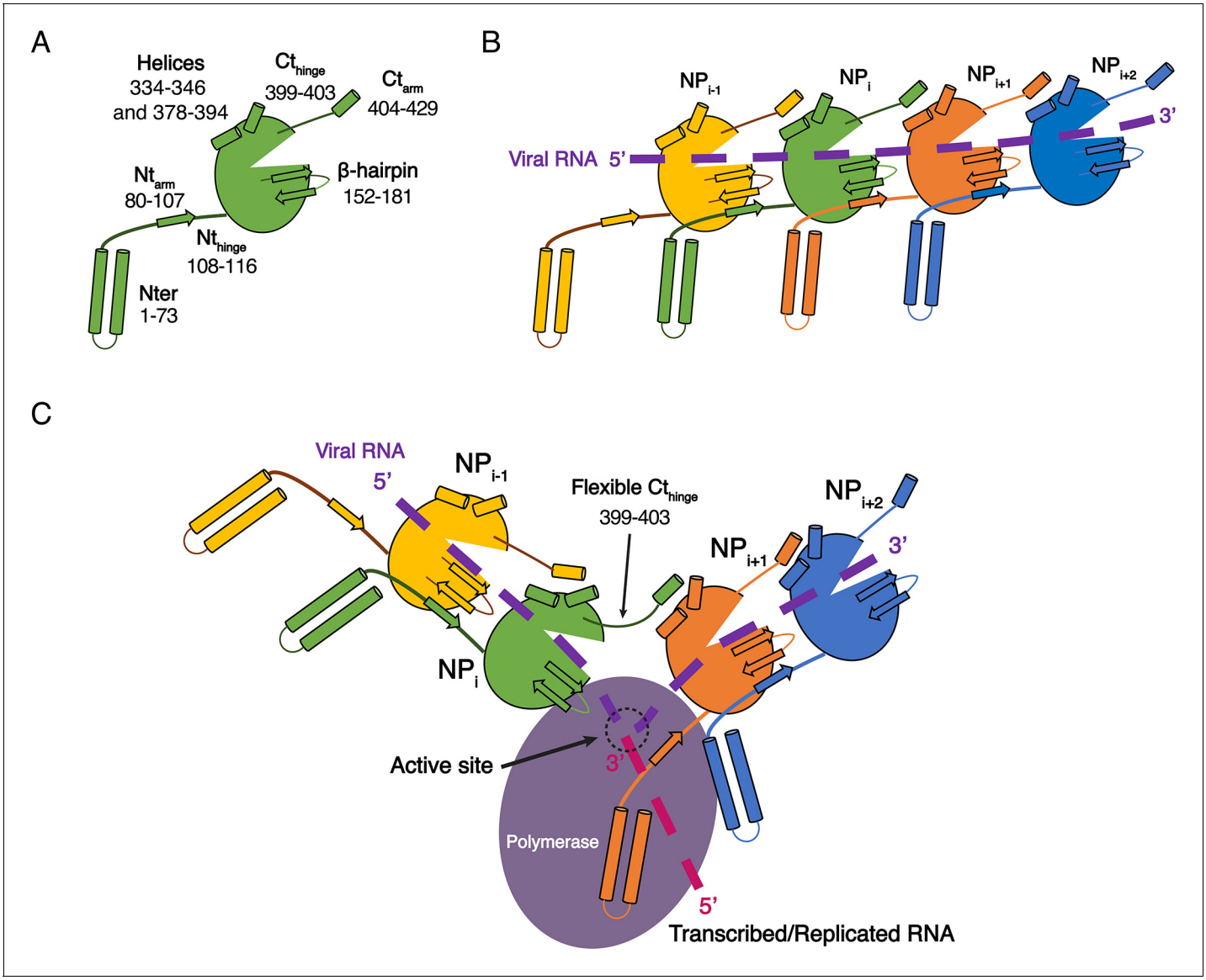

Figure 4. Model of HTNV replication and transcription. (**A**) Schematics representation of HTNV-NP. Major secondary structures involved in interprotomer interactions are represented as arrows for β-strand and cylinders for α-helices. RNA binding cavity is represented as a clipped part from the NP_{core} region (green oval). (**B**) Schematic representation of RNA binding and NP-NP interactions. RNA is shown as a dotted purple line. Main NP-NP interactions between adjacent subunits are indicated. For clarity, NP_i interactions with NP_{i-2}, NP_{i-3}, NP_{i+2} and NP_{i+3} are absent from the schematic representation. (**C**) Replication working hypothesis model which is inspired from ***Gerlach et al. (2015)***. The polymerase is shown in purple and the newly transcribed/replicated RNA is indicated as a pink dotted line. The model proposes that the polymerase binds to the flexible N-terminal$_{1-73}$ region during replication/transcription in order to move along the NC. This would be reminiscent to P and L binding to flexible sNSV C-terminal region. Binding of the polymerase to the N-terminal$_{1-73}$ region could destabilise the adjacent Nt_{arm} binding. This localised disruption of NP-NP interaction would create a local opening of the NC enabling transient access of the polymerase to few RNA nucleotides for replication/transcription. Such an opening could be possible without disturbing the whole NC as NP to NP contacts are driven not only by the Nt_{arm} but also by the Ct_{arm}. The Ct_{arm} interaction is likely to remain intact even with a local opening of the NC as the C-terminal hinge allows the Ct_{arm} to undergo large rotation.
DOI: https://doi.org/10.7554/eLife.43075.014